Modelling the growth stress in tree branches: eccentric growth vs. reaction wood

A van Rooij, Eric Badel, Jean-François Barczi, Yves Caraglio, Tancrede Almeras, Joseph Gril

▶ **To cite this version:**

A van Rooij, Eric Badel, Jean-François Barczi, Yves Caraglio, Tancrede Almeras, et al.. Modelling the growth stress in tree branches: eccentric growth vs. reaction wood. Peer Community Journal, 2023, 10.24072/pcjournal.308 . hal-03748026v4

HAL Id: hal-03748026

https://hal.science/hal-03748026v4

Submitted on 13 Jan 2023 (v4), last revised 21 Nov 2023 (v6)

HAL is a multi-disciplinary open access archive for the deposit and dissemination of scientific research documents, whether they are published or not. The documents may come from teaching and research institutions in France or abroad, or from public or private research centers.

L'archive ouverte pluridisciplinaire **HAL**, est destinée au dépôt et à la diffusion de documents scientifiques de niveau recherche, publiés ou non, émanant des établissements d'enseignement et de recherche français ou étrangers, des laboratoires publics ou privés.

Modelling the growth stress in tree branches: eccentric growth *vs.* reaction wood

A. Van Rooij[1,2], E. Badel[2], J.F. Barczi[3], Y. Caraglio[3], T. Alméras[4] and J. Gril[1,2]

1. Université Clermont-Auvergne, CNRS, Institut Pascal, F-63000, Clermont-Ferrand, France
2. Université Clermont-Auvergne, INRAE, PIAF, F-63000, Clermont-Ferrand, France
3. CIRAD, UMR AMAP, F-34398 Montpellier, France.
AMAP, Univ Montpellier, CIRAD, CNRS, INRAE, IRD, Montpellier, France.
4. LMGC, CNRS, Université of Montpellier, Montpellier, France

Abstract

This work aims to model the mechanical processes used by tree branches to control their posture despite their increasing weight loading. The two known options for a branch to maintain its orientation are the asymmetry of maturation stress, including reaction wood formation, and eccentric radial growth. Both options can be observed in nature and influence the stress distribution developed in the branch each year. This so-called "growth stress" reflects the mechanical state of the branch. In this work, a growth stress model was developed at the cross-section level in order to quantify and study the bio-mechanical impact of each process. For illustration, this model was applied to branches of two 50-year-old trees, one softwood *Pinus pinaster* and one hardwood *Prunus avium*, both simulated with the AMAPSim finite element software. The computed outputs enlightened that, for both *Prunus avium* and *Pinus pinaster*, eccentric radial growth is less efficient than the formation of reaction wood to counter increasing gravity stress applied to the branch. For the pine, although eccentric growth does not necessarily act as a relevant lever for postural control, it greatly modifies the profile pattern of mechanical stress and could provide mechanical safety of the branch. This work opens experimental perspectives to understand the biomechanical processes involved in the formation of branches and their mechanical safety.

Abbreviations and notations (in order of occurrence)

NW,TW,CW	Normal Wood, Tension Wood, Compression Wood
(x, y, z)	Local reference coordinates associated with the section
O	Centre of the section
r, R	Radial polar coordinate and Radii of the cross section (m)
$e(R), \overline{e(R)}$	Eccentricity at the stem radius R, integrated eccentricity up to r = R
(x', y', z')	Local reference coordinates associated with the section, centred on the pith
σ	Stress (MPa)
σ_0	Induced maturation stress (Mpa)
S	Cross section area (m^2)
N, M	Loads (N): normal force parallel to z' and bending moment around y'
E	Module of elasticity in L direction (GPa): MOE
μ	Induced maturation strain
ϵ, a, b	Strain, at the center, local curvature
K_i	Structural stiffness of the cross-section
F_i	External coefficients (maturation and load)
θ	Circumferential position in section (rad)
$\sigma_0(\theta)$	Maturation strain in the new ring at circumferential position θ
α	Mean maturation stress in the new ring
β	Differential stress in the new ring
$R_{x'y'}$	Radius of the cross section at the instant of appearance of the point (x', y')
$\lambda_N, \lambda_M, \nu_M, \nu_N$	Load power law: allometric coefficient
λ_b, ν_b	Change of curvature power law: allometric coefficient
$\sigma_{NW}, \sigma_{TW}, \sigma_{CW}$	Maturation stress in the normal wood, tension wood and compression wood
$\mu_{NW}, \mu_{TW}, \mu_{CW}$	Maturation strain in the normal wood, tension wood and compression wood
$\overrightarrow{N_n}, \overrightarrow{M_n}$	Loads of growth unit n: normal force and bending moment around y
N_z, M_x, M_y, M_z	Loads of growth unit n: projection of $\overrightarrow{N_n}$ on $\vec{z}$ and bending moment $\overrightarrow{M_n}$ around $\vec{x}, \vec{y}, \vec{z}$
m_n	Mass of the growth unit n (kg)
g	Gravity constant: $g = 9.8$ m.s^{-2}
G_n	Centre of gravity of the growth unit n
E_d, E_g	Air-dry, green MOE
ρ	Density
μstrain	$1/10^6$
D_n, D_{n+1}	First and second diameter the growth unit n
D_f	Deflection of a growth unit
L_n	Length of the growth unit n

Introduction

From a mechanical point of view, wood in tree fulfils three major functions: construction of the tree architecture, postural control of trunk and branches and breaking resistance to external stimuli [Thibaut (2019)]. These three functions are provided by the way wood cells differentiate and accumulate during wood formation process. Each axis of a tree can be considered as an inclined beam, consisting of a succession of conical growth units [Barthélémy and Caraglio (2007)]. It is built in two steps: first, primary growth resulting in new growth units that increase the length of the initial axis; and secondary growth resulting in thickening of already existing units by addition of annual rings. These two interactive and additional processes lead to a specific pattern of mechanical stress, called 'growth stress', which can be analysed as the superposition of support stress and maturation stress [Archer (1976); Fournier et al. (1991a)]. The

support stress results from the continuous increase of the weight supported by the axis over the years. It reaches maximal levels in the core of the stem and vanishes near stem periphery, where the recently formed wood contributes to the support of recently produced biomass only. Maturation stress is set up at the end of the cell-wall maturation process, when molecular components such as lignin polymerise, generating growth forces by small dilatation or contraction restrained by the rigidity of the previously formed wood cells [Alméras and Clair (2016)]. An evaluation of the maturation stress can be obtained by measuring the strain associated to stress release at stem periphery, where no support stress is present [Nicholson (1971); Yoshida and Okuyama: (2002); Yang et al. (2005)]. The circumferential heterogeneity of this peripheral stress is needed to regulate stem curvature. In most cases, a tensile maturation stress is produced in the newly formed 'normal wood' (NW). But observations on inclined trunks [Alméras et al. (2005); Coutand et al. (2007); Thibaut and Gril (2021)], seedlings [Hung et al. (2016)] and branches [Fisher and Stevenson (1981); Huang et al. (2010); Tsai et al. (2012); Hung et al. (2017)] have evidenced a clear difference between hardwood and softwood behaviour. Hardwoods are able to produce 'tension wood' (TW) inducing a much higher tensile stress on one side, while for softwood a compressive stress is induced in 'compression wood' (CW). The first pulls, the second pushes. In the most usual case of inclined stems restoring their vertical orientation, TW is formed on the upper side while CW is formed on the lower side of the trunk. But other situations can be encountered depending on the biomechanical requirements of the tree [Wang et al. (2009b)]. In addition to their participation in the postural control of tree stems, these two types of so-called 'reaction wood' (RW) are characterised by specific anatomical pattern (not discussed here) and specific physical and mechanical properties.

As an alternative to complex experimental approaches, growth stress modelling plays an important role in the understanding of the phenomena involved in the orientation process of a stem. The history of biomechanical models began with Kübler (1959) who proposed an analytical formulation of growth stress for a perfect cylinder made of a homogeneous and transversally isotropic wood. Later, Archer and Byrnes (1974) took into account an asymmetry of the maturation stress, and Fournier et al. (1991a,b) proposed a semi-incremental version of these models, allowing to take into account a potential gradient of mechanical parameters (stiffness, maturation).
By associating their previous model to the loading induced by the tree weight, Fournier et al. (1994) made the connection between growth stress and stem orientation. This model has been adopted and developed by several authors in order to study the orientation process of stems. Yamamoto et al. (2002) added a primary shoot and returned to curvature calculations. Alméras and Fournier (2009) introduced the notion of gravitropic performance (capacity of the tree to correct the bending moment induced by its weight) and proposed criteria of long-term stability. Huang et al. (2005) and Alméras et al. (2005) impoved the model by introducing a secondary growth asymmetry and its resulting pith eccentricity, as well as stiffness heterogeneity, allowing to quantify the effectiveness of eccentricity, maturation, stiffness gradient and initial radius in the curvature regulation process. They enlightened that the main factor in the gravitropic process is the spatial distribution of the maturation stress. Still in line with Fournier's 1994 model, Alméras et al. (2018) recently developed analytical models of longitudinal growth stress, taking into account different configurations, like eccentricity or maturation gradient, and evolution laws, like evolution of stiffness per additional layer. Finally, based on the same philosophy as established by Kübler, tree-scale and finite-element models have emerged [Fourcaud et al. (2003); Ancelin et al. (2004)].

Huang et al. (2010)'s model has been used to understand how eccentric growth and RW are involved in branch orientation [Wang et al. (2009a); Huang et al. (2010); Tsai et al. (2012); Hung et al. (2017)], but all theses studies were based on the current state of the branch, without consideration of the previous history: although some of them quantified the roles of maturation and eccentricity in the regulation of curvature, none did evaluate their capacity to ensure a given growth scenario.

Unlike trunks, which usually seek verticality, after the first stages of growth, branches tend to grow in a stationary way at a fixed angle to the vertical. Therefore, in this framework, we focus on understanding

how branches can control their orientation, through the study of two growth parameters: eccentric growth and RW. The aim is to check by calculation what option is mechanically possible and safe for the branch. For this purpose, we developed a semi-incremental biomechanical model of growth stress at the cross section level that takes into account the eccentricity and maturation gradients during the construction of branches. Using the digital models of one softwood *Pinus pinaster* and one hardwood *Prunus avium*, the impact of each of these two growth parameters on the stress state was evaluated.

Material and methods

Numerical model

General hypotheses

The problem was set in the framework of the beam theory. From a geometrical point of view, branches generally show profiles that suit to this type of analytical framework: a slender shape and no important diameter variations. The shape effects due to twigs and other local biological phenomena (cavity, nodes, etc.) were neglected. The same set of hypotheses as in Alméras et al. (2018) was adopted. In this study, we focused on the behaviour in the longitudinal direction (parallel to the main axis). Horizontal bending and torsion loads were not considered. Only the vertical bending moment (caused by the weight) was considered; these hypotheses on the loading modes are discussed later.

Geometrical settings

The object of study was the cross-section of a branch, placed within a plane locally orthogonal to the pith. The local reference frame of the section is $(\vec{x}, \vec{y}, \vec{z})$, with $\vec{z}$ the longitudinal direction of the axis, and $\vec{x}$ placed in a vertical plane and facing upwards (Fig 1). The shape of the cross-section was assumed to be circular at any stage of development, described by the successive depositions of wood rings. The term of 'ring' refers here to the volume occupied by wood cells produced by the cambium during a certain duration of time, not necessarily annual: it must be taken in a numerical meaning. These rings possibly could present an eccentricity resulting from asymmetry of secondary growth. Since the model only takes into account vertical bending, the eccentricity was set along the x axis, as expressed by the following equation:

$$O(t) = \int_0^{R(t)} e(r)dr = \overline{e}R(t) \tag{1}$$

with $O(t)$ the position of the geometrical centre and $R(t)$ the radius of the section at time t, e(r) the eccentricity when the stem radius was r and $\overline{e}$ the integrated eccentricity up to $r = R$. The eccentricity can vary in the interval $[-1, 1]$. A zero eccentricity corresponds to a centred section, while -1 or 1 corresponds to maximum eccentricity resulting from secondary growth only on the lower or the upper side of the section, respectively. In the following, the position x' in the pith reference frame is needed. By calling x the vertical position in the geometrical reference frame, we deduce from equation (1):

$$x = x' - \overline{e}R \tag{2}$$

Computation of the mechanical behaviour

We developed a radial incremental method. For each radial increment, the longitudinal stress was computed in order to satisfy the static equilibrium of the cross section:

$$\begin{cases} \int_S \delta\sigma dS + \int_{\delta S} \sigma_0 dS = \delta N & \text{(3a)} \\ \int_S \delta\sigma x dS + \int_{\delta S} \sigma_0 x dS = -\delta M & \text{(3b)} \end{cases}$$

where S is the cross-section area, δS is its increment, $\delta\sigma$ is the increment of stress σ in the already formed wood, in response to the maturation stress σ_0 generated in the new wood layer. δN and δM are respectively the increment of external force N and bending moment M, that are applied on the cross-section. For illustration, the geometric situation for K rings and an increment of stem radius δR is proposed in Fig 1.

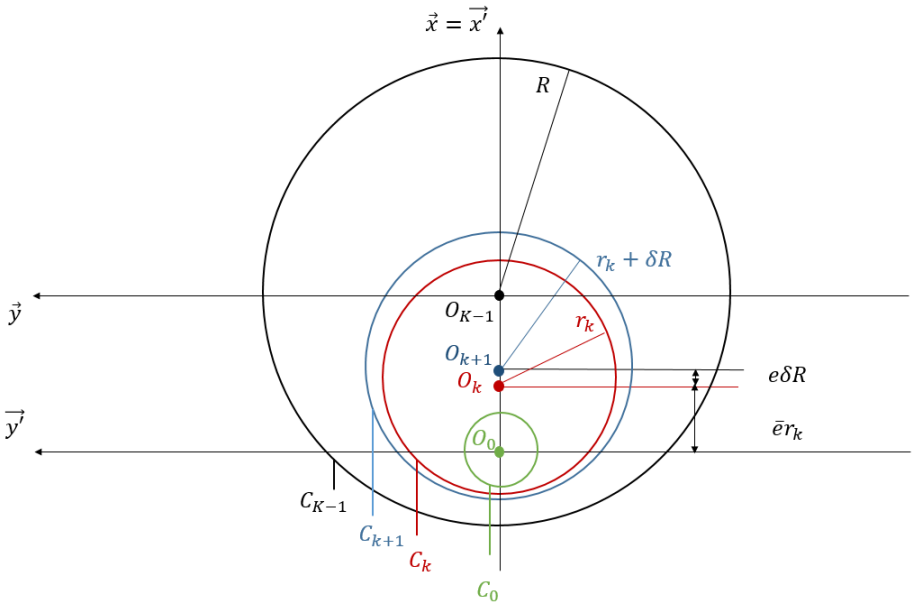

Figure 1: Geometrical representation of a section with K numerical rings and a radial increment δR between rings $(k-1)$ and k.

The stress σ is linked to the strain ϵ by a classical pre-stressed Hooke's law:

$$\sigma = E\left(\epsilon - \mu\right) = E\epsilon + \sigma_0 \tag{4}$$

where E is the longitudinal Young's modulus, μ is the maturation strain and σ_0 is the maturation stress. In the context of the beam theory, the planar cross-sections remain so (Euler-Bernouilli assumption). The strain field is then described by the deformation a at the centre of the pith and the curvature b relative to the y-axis, as follows:

$$\delta\epsilon = \delta a + x\delta b \tag{5}$$

where $\delta\epsilon$, δa, δb are the increments of ϵ, a, b, respectively. The stress increment $\delta\sigma$, in the already formed wood, where no maturation occurs anymore, can then be deduced:

$$\delta\sigma = E\delta\epsilon = E(\delta a + x\delta b) \tag{6}$$

From these considerations, the system (3) becomes (details of the calculation are given in Appendix A):

$$\begin{cases} K_0\delta a + K_1\delta b = \delta F_0 & \text{(7a)} \\ K_1\delta a + K_2\delta b = \delta F_1 & \text{(7b)} \end{cases}$$

with

$$K_0 = E\pi R^2, \quad K_1 = E\pi\bar{e}R^3, \quad K_2 = E\pi R^4\left(\bar{e}^2 + \frac{1}{4}\right) \tag{8}$$

$$\delta F_0 = -\int_{\delta S}\sigma_0 dS + \delta N, \quad \delta F_1 = -\int_{\delta S}\sigma_0 x dS - \delta M$$

The calculation of the coefficients δF_0 and δF_1 depends on the formulation of the maturation stress. The maturation stress was assumed to vary circumferentially as follows:

$$\sigma_0(\theta) = \alpha + \beta \cos\theta \tag{9}$$

where the mean stress α and differential stress β were defined differently in softwood and hardwood species:

$$\begin{cases} \text{Hardwood: } \alpha = \dfrac{\sigma_{TW} + \sigma_{NW}}{2}; \beta = \dfrac{\sigma_{TW} - \sigma_{NW}}{2} & \text{(10a)} \\ \text{Softwood: } \alpha = \dfrac{\sigma_{CW} + \sigma_{NW}}{2}; \beta = \dfrac{\sigma_{NW} - \sigma_{CW}}{2} & \text{(10b)} \end{cases}$$

σ_{TW} (resp. σ_{CW}) being the maturation stress in the TW (resp. CW), and σ_{NW} that in the opposite wood (NW). One gets :

$$\begin{cases} \delta F_0 = -\pi R \left(2\alpha + e\beta\right) \delta R + \delta N & \text{(11a)} \\ \delta F_1 = -\pi R^2 \left(3\alpha e + e^2\beta + \beta\right) \delta R - \delta M & \text{(11b)} \end{cases}$$

From equations (8), (11a) and (11b), the components of the system (7) are known. By inversion, $\delta\alpha$ and δb can be obtained according to the following equations (see details in Appendix B):

$$\begin{cases} \delta a = \dfrac{4}{ER}\left[\left(3e\overline{e} - 2e^2 - \dfrac{1}{2}\right)\alpha + \left(\overline{e}e^2 - e\overline{e}^2 + \overline{e} - \dfrac{e}{4}\right)\beta\right]\delta R + \dfrac{4}{E\pi R^3}\left[\overline{e}\delta M + \left(\overline{e}^2 + \dfrac{1}{4}\right)R\delta N\right] & \text{(12a)} \\ \delta b = \dfrac{-4}{ER^2}\left[\left(3e - 2\overline{e}\right)\alpha + \left(e^2 - e\overline{e} + 1\right)\beta)\right]\delta R - \dfrac{4}{E\pi R^4}\left(\delta M + \overline{e}R\delta N\right) & \text{(12b)} \end{cases}$$

Once δa and δb are known, the stress increment $\delta\sigma$ at any position given by (x', y') can be obtained from equation(6). The stress distribution at this position can be obtained as the sum of the initial maturation stress and all the stress increments undergone by the material point since its creation.

$$\sigma(x', y', R) = \sigma_0(x', y') + \sum_{k=k_{x'y'}}^{K} \delta\sigma_k \tag{13}$$

where $\delta R_k = r_k - r_{k-1}$ for a succession of ring radii $0 < r_0 < ... < r_k < ... < r_K = R$, $\delta\sigma_k$ is the corresponding increment, and $k_{x'y'}$ designates the ring containing the point.

Analytical formulations

Using equations (12b) and dividing by δR, we get the following equations when δR tends to zero :

$$\begin{cases} \dfrac{\mathrm{d}a}{\mathrm{d}R} = \dfrac{4}{ER}\left[\left(3e\overline{e} - 2e^2 - \dfrac{1}{2}\right)\alpha + \left(\overline{e}e^2 - e\overline{e}^2 + \overline{e} - \dfrac{e}{4}\right)\beta + \dfrac{1}{\pi R^2}\left(\overline{e}\dfrac{\mathrm{d}M}{\mathrm{d}R} + \left(\overline{e}^2 + \dfrac{1}{4}\right)R\dfrac{\mathrm{d}N}{\mathrm{d}R}\right)\right] & \text{(14a)} \\ \dfrac{\mathrm{d}b}{\mathrm{d}R} = \dfrac{-4}{ER^2}\left[\left(3e - 2\overline{e}\right)\alpha + \left(e^2 - e\overline{e} + 1\right)\beta + \dfrac{1}{\pi R^2}\left(\dfrac{\mathrm{d}M}{\mathrm{d}R} + \overline{e}R\dfrac{\mathrm{d}N}{\mathrm{d}R}\right)\right] & \text{(14b)} \end{cases}$$

Using equation (13) and dividing again by a vanishing δR, we obtain the following equation involving the partial derivative $\partial\sigma/\partial R$:

$$\sigma(x', y', R) = \sigma_0(x', y') + \int_{R_{x'y'}}^{R} \frac{\partial\sigma}{\partial R}(x', R')dR' \tag{15}$$

where $R_{x'y'}$ is the radius of the section at the instant of appearance of the point with coordinates (x', y').

On the other hand, the expressions of axial force $N(R)$ and bending moment $M(R)$ are required to compute the evolution of the stress distribution in the cross section. For this purpose, we assumed that both vary as a power function of the radius of the branch. This resulted in the following allometric laws:

$$\begin{cases} N = \lambda_N R^{\nu_N} & \text{(16a)} \\ M = \lambda_M R^{\nu_M} & \text{(16b)} \end{cases}$$

wehre $\lambda_{N,M}$ and $\nu_{N,M}$ are allometric coefficients. The $\lambda-$coefficients are directly proportional to the weight of the branch part supported by the cross section (the branch itself and the other axes of higher orders). The $\nu-$coefficients express the kinetics of the secondary growth: a small ν refers to an early secondary growth while a higher one refers to a later diameter increase.

The calculation of σ requires also the knowledge of the temporal variation of the curvature b. In order to simplify the analyses, we mainly studied stationary cases, i.e. we assumed that the branch maintains its orientation and remains straight. This assumption results in $\dfrac{\mathrm{d}b}{\mathrm{d}R} = 0$. Physiologically, this equation expresses that the branch always compensates its weight increment at each deposition step of a new wood layer, corresponding to an additional weight. However, we can consider two cases for which the branch does not build up in a stationary way: i) the passive bending (under its own weight) case, and ii) the up-righting case (i.e. the action of maturation is stronger than the additional weight). In both cases, the resulting change in curvature has been modelled by Alméras and Fournier (2009) and Alméras et al. (2018). It can then be written as follows:

$$\begin{cases} \text{Up-righting:} & \dfrac{\mathrm{d}b}{\mathrm{d}R} = -4\dfrac{\beta}{ER^2} & \text{(17a)} \\ \text{Passive bending:} & \dfrac{\mathrm{d}b}{\mathrm{d}R} = 4\dfrac{\lambda_M \nu_M}{E\pi} R^{\nu_M - 5} & \text{(17b)} \end{cases}$$

For the next computations, we used the following general law:

$$\frac{\mathrm{d}b}{\mathrm{d}R} = \lambda_b R^{\nu_b} \tag{18}$$

As a remark, even if this equation bears some resemblance to (16), it does not express any notion of allometry and is used here only for convenience. Combining (14),(15),(16) and (18), the total stress can then be computed as:

$$\sigma^i(x', y', R) = \sigma_0^i(x', y') + S_1 \ln\left(\frac{R}{R_{x'y'}}\right) + \frac{S_2}{S_3}\left(R^{S_3} - R_{x'y'}^{S_3}\right) + \frac{S_4}{S_5}\left(R^{S_5} - R_{x'y'}^{S_5}\right) + \frac{S_6}{S_7}\left(R^{S_7} - R_{x'y'}^{S_7}\right) x' \tag{19}$$

where $S_1 = 4\left[\left(3e\overline{e} - 2e^2 - \frac{1}{2}\right)\alpha + \left(\overline{e}e^2 - e\overline{e}^2 + \overline{e} - \frac{e}{4}\right)\beta\right]$ is driven by the maturation process, $S_2 = \frac{\lambda_N \nu_N}{\pi}\left(\overline{e}^2 + \frac{1}{4}\right)$, $S_3 = \nu_N - 2$, $S_4 = \frac{4}{\pi}\lambda_M \nu_M \overline{e}$ and $S_5 = \nu_M - 3$ by the branch loading (geometric evolution of the branch), $S_6 = E\lambda_b$ and $S_7 = \nu_b + 1$ by the branch orientation.
For each radius r, the remaining unknowns are the mean stress α, the differential stress β and the eccentricity e. Equation (14b) can be rewritten as:

$$(3e - 2\overline{e})\,\alpha + \left(e^2 - e\overline{e} + 1\right)\beta = \frac{-1}{\pi r^2}\left(\frac{dM}{dR} + \overline{e}R\frac{dN}{dR}\right) - E\frac{R^2}{4}\frac{db}{dR} \tag{20}$$

Thus by fixing two parameters, the third is directly determined. The maturation parameters α and β are determined by the maturation stress σ_{NW} in NW and σ_{TW} or σ_{CW} in RW according to equation (10).
We considered two possible configurations for the simulations in next section:

1. First, we applied a constant eccentricity (so that $\bar{e} = e$) and we fixed the stress level in the NW. In that case, the maturation stress of the RW was given by equations (10):

$$\begin{cases} \sigma_{TW} = \dfrac{-2}{\pi R^2(1+e)}\left(\dfrac{dM}{dR} + er\dfrac{dN}{dR}\right) + \sigma_{NW}\left(\dfrac{1-e}{1+e}\right) + \lambda_b\left(\dfrac{ER^2}{2(1+e)}\right)R^{\nu_b} & \text{(21a)} \\ \sigma_{CW} = \dfrac{2}{\pi R^2(1-e)}\left(\dfrac{dM}{dR} + eR\dfrac{dN}{dR}\right) + \sigma_{NW}\left(\dfrac{1+e}{1-e}\right) - \lambda_b\left(\dfrac{ER^2}{2(1-e)}\right)R^{\nu_b} & \text{(21b)} \end{cases}$$

2. Second, we fixed the maturation parameters and we observed how the eccentric growth could, or not, maintain the orientation of the branch. In this configuration, equation (20) became a two degrees equation in e that could be solved numerically.

In these two configurations, using data on the support allometries $\lambda_N, \lambda_M, \nu_M, \nu_N$, we can calculate the stress in the RW and/or the eccentricity with different (λ_b, ν_b), then deduce the growth stress profile in the section (eq. 19). In the next part, we see how the allometric coefficients can be obtained from data generated by growth model.

Realistic growth data

Tree architecture modelling

Numerical experiments were carried out using two reference models: one softwood *Pinus Pinaster* (pine) and one hardwood *Prunus avium* (birch) (Fig 2). Their growth follows the architectural model of Rauh [Hallé et al. (1978)]. This implies that the branching is rhythmic, the axes are monopodial and the branches are orthotropic. These digital trees were computed with AMAPSim software [Barczi et al. (2007)]. The input of this software are architectural parameters which were provided by observations and field studies: Coudurier et al. (1993) and Heuret et al. (2006) for *Pinus pinaster*, Caraglio (1996) and Barthélémy et al. (2009) for *Prunus avium*. The choice of theses species was based on the availability of temperate species in AMAPSim database. The two trees were modelled over 50 years in open-growth conditions, which did not correspond to the same ontogenic stage of development, but allowed both trees to be considered mature. In the final state, the pine (resp. birch) was 18,2 m (resp. 14,1 m) high. The diameter at the base was 40 cm for both species. The insertion height of the first branch was 14,3 m for pine and 4,6 m for the birch. The branches of interest were the main branches; those that were directly attached to the trunk. In addition, only branches that were more than 20 years old have been studied, so that they had a consistent loading history. Finally, 33 branches for the pine and 45 for the birch were selected. For each of the branch groups, the distributions of length L, radius r and insertion angle with the trunk θ are shown in Table 1.

Species	L_m (m)	r_m (m)	θ_m (°)
Pinus pinae	5.3 ± 0.4	5.2 ± 0.3	70 ± 0.01
Prunus avium	7.9 ± 1.4	8.1 ± 0.7	80 ± 0.05

Table 1: Geometric distribution of branches of interest

.

Loading scenarii: allometric laws

Each tree was composed of axes organised hierarchically according to their order: 1 for the tree seed, 2 for the trunk, 3 for the main branches, 4 for those attached to them, etc.. Each axis was described as a succession of growth units (GU), which were sections of cones, identified by a number (in order of appearance), and defined by a parent number, an order, a start and end diameter, the coordinates of the centres of both initial and final sections as well as their length (Fig 3). Note that the description provided by AmapSim did not include the internal structure of the growth units, such as eccentricity. To avoid

(a) (b)

Figure 2: AMAPSim representation of aerial architecture of 50-years old trees. (a) *Prunus avium* and (b) *Pinus pinaster*

unnecessary complications, the coordinates of the centres were taken as those of the pith. From the model data, the moments and normal forces can be computed in each growth unit, at any time of the tree's existence. In addition to a part of its own weight, each unit is subjected to the weight of its offsprings - this term referring to any growth unit that would fall if the studied one was cut. The normal force $\overrightarrow{N_n}$ and bending moment $\overrightarrow{M_n}$ supported by the growth unit n can be written:

$$\overrightarrow{N_n} = \frac{1}{2} m_n \vec{g} + \sum_{\substack{k \succ n \\ k \ offspring}} m_k \vec{g} \tag{22}$$

$$\overrightarrow{M_n} = \overrightarrow{G_n G'_n} \wedge \left(\frac{1}{2} m_n \vec{g} \right) + \sum_{\substack{k \succ n \\ k \ offspring}} \overrightarrow{G_n G_k} \wedge (m_k \vec{g}) \tag{23}$$

where G_n is the centre of gravity of the current growth unit, G'_n is the centre of gravity of its second half. On the downstream side of G_n, G_k is the centre of gravity of an offspring of number $k > n$, m_i is the mass of growth unit i and $\vec{g}$ is the gravity vector. Once $\overrightarrow{N_n}$ and $\overrightarrow{M_n}$ were computed in the absolute coordinates used for the description of the whole tree, they were projected in the local coordinates system $(\vec{x'}, \vec{y'}, \vec{z})$, with $\vec{z}$ of the chosen cross section. In the following, in accordance with the development of the previous section, N_z refers to the projection of $\overrightarrow{N}$ on $\vec{z}$ and M_y to the projection of $\overrightarrow{M}$ on $\vec{y'}$.

Power law regressions were performed to recover the allometric coefficients $\lambda_M, \lambda_N, \nu_N, \nu_M$. A summary of the analysis process is proposed in Fig 3.

For the selected branch groups, the distribution of all allometric coefficients are presented in Fig 4. In *Pinus*, there was a large variation in $\nu-$coefficient, with ν_M varying by almost a factor 2 in the studied sample; indicating very variable secondary growth kinetics. In *Prunus*, the range of variation of the allometric power coefficients was smaller, which depicted a higher homogeneity of secondary growth kinetics. For both species, a great diversity in $\lambda-$ coefficients was observed, which depicted a significant variability in the loading history. This is particularly interesting as the branches showed geometric determinants that did not vary over large ranges (Table 1). Also, these coefficients do not appear to vary as a function

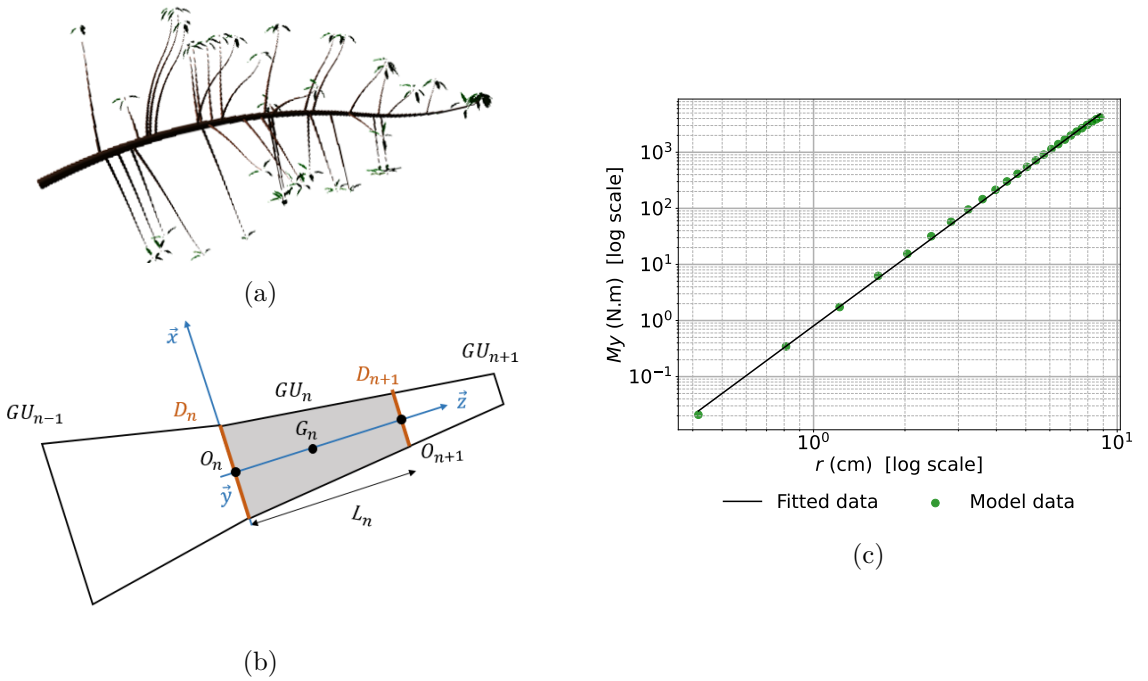

Figure 3: Allometric law of *Prunus avium*. The bending moment is calculated from the geometry of the modelled branch (a) and (b). The graph (c) represents the relationship between the branch diameter and the bending moment. The fitted curve provides the allometric law.

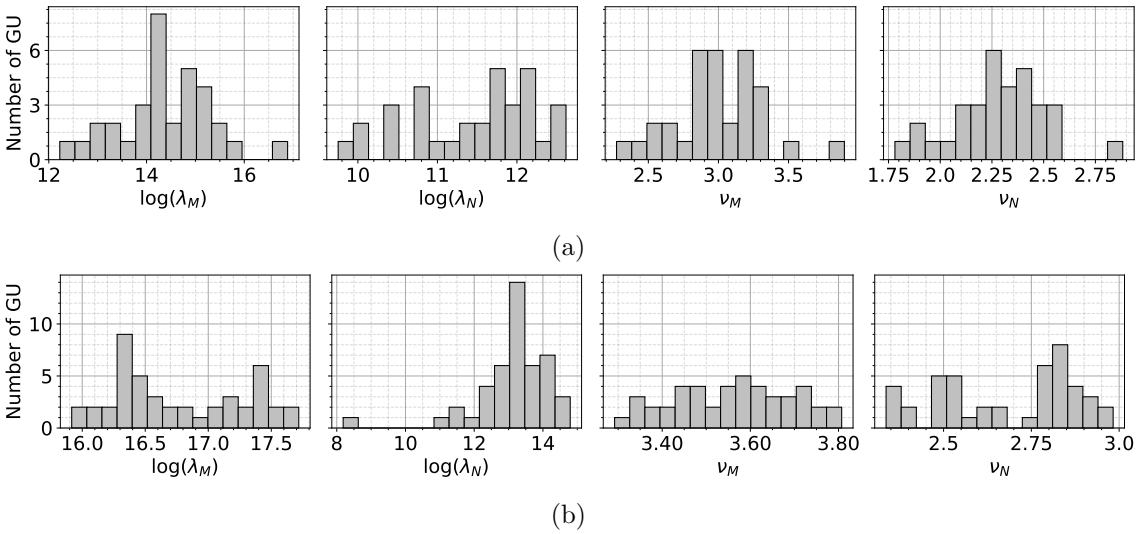

Figure 4: Statistical distribution of allometric coefficients for modelled branches: (a) *Pinus pinaster* (b) *Prunus avium*. $\lambda_{M,N}$ refers to the weight, $\nu_{M,N}$ to the kinetic of secondary growth.

of geometric parameters. This reflects the complexity of predicting the loading of a branch from the determinants of the main axis, and shows the importance of branching. In both cases, these variations in the $\lambda-$coefficients result in a factor of 4 in the bending load between the lightly loaded and the heavily loaded branches.

The average values of each allometric and final geometry, indicated in table 2, will be used for the simulations.

Material data

The stress values in the NW were fixed according to the average maturation strains advised by Thibaut and Gril (2021). Similarly, the green wood MOE were given by the correlation between dry and green MOE identified by Thibaut and Gril (2021): $Eg = 0.89 * Ed$. Dry MOE were provided by the tropix database of CIRAD [Gérard et al. (2011)]. The density of green wood was approximated by the density of water $\rho = 1000\ kg.m^{-3}$. These inputs are summarised in Table 2.
In the following section, the case of stationary growth ($\nu_b = 0$) will be considered principally and analysed thoroughly. Situations of changing curvature will be then considered briefly.

Species	λ_M	λ_N	ν_M	ν_N	r	μ_{NW}	E_d	E_g
Pinus pinae	-6.4e6	5e4	3.2	2.5	0.05	410	8.8	7.9
Prunus avium	-2.6e7	9.5e3	3.6	2.7	0.08	712	10.2	9.1

Table 2: Mean input characteristics of the branches.$\lambda_{N,M}$ and $\nu_{N,M}$ correspond to the allometric evolution of the normal load and bending moment, r (m) is the radius at the basal part of the branch, ν_{NW} (μstrain) is the maturation strain in the NW, and $E_{d,g}$ (GPa) is the dry and green modulus of the material.

Results

Prunus avium

Fig 5 shows simulation results obtained for *Prunus avium*, when one of the factors (eccentricity or RW) is set to zero. On Fig 5.a, the stress on the whole section is represented. In this case, the branch maintains its orientation through the formation of RW only (no eccentric growth). The area near the pith is in compression (red), while the periphery is in tension (blue), with a higher tension on the upper side, allowing to maintain the orientation. Fig 5.b shows the interpolation of the stress distribution of Fig 5.a on the main axis y=0. The Fig 5.c represents the maturation stress in the TW throughout the growth of the branch. The larger the branch grew, the higher the needed stress level. The symmetric case, with no formation of RW but eccentric growth, is presented in Fig 5.d-f. This example illustrates that eccentricity alone could theoretically provide the orientation control. Fig 5.f shows the evolution of the eccentricity through the radial growth of the branch. Like the RW stress in the previous case, the needed eccentricity increased when the branch grew. The pattern of stress distribution of Fig 5.d is quiet similar as in Fig 5.a , with compression near the pith and tension at the periphery, but the section is off-centred and the tension at periphery is the same all around the section, confirming the absence of RW.

Fig 6 shows the combination of the two factors. For each of them, three different scenarii were proposed. In Fig 6.a, the RW factor controlled the orientation. Different eccentricities, ranging from -0.5 to 0.5 were imposed. The resulting stress patterns are represented in Fig 6.a.i : the higher tension on the upper side maintained the posture. The more hypotrophic the eccentricity, the higher the tension stress at periphery. This is confirmed by the evolution of RW maturation stress through branch growth in Fig 6.a.ii. The situations where the eccentricity controlled the posture are shown in Fig. 6.b. Where uniform tension was imposed ($\sigma_{TW} = 2\sigma_{NW}$, $\sigma_{TW} = 3\sigma_{NW}$), the eccentricity pattern became particular: we observed a decrease during the first year, followed by an increase (Fig 6.b.ii). This is explained by the growth scenario: at the beginning of the development, fixing a uniform RW formation tended to right-up the stem, while a stationary orientation was imposed. Therefore, the eccentricity process counteracted this righting up movement, leading to the initial decrease. As the branch grew, the effect of the RW decreased and the branch tended to bend forward: the eccentricity counteracted this trend, leading to the final increase. This coordination problem may probably be specific to our scenario that imposed a stationary orientation throughout the entire growth the branch, including the first stages of development.

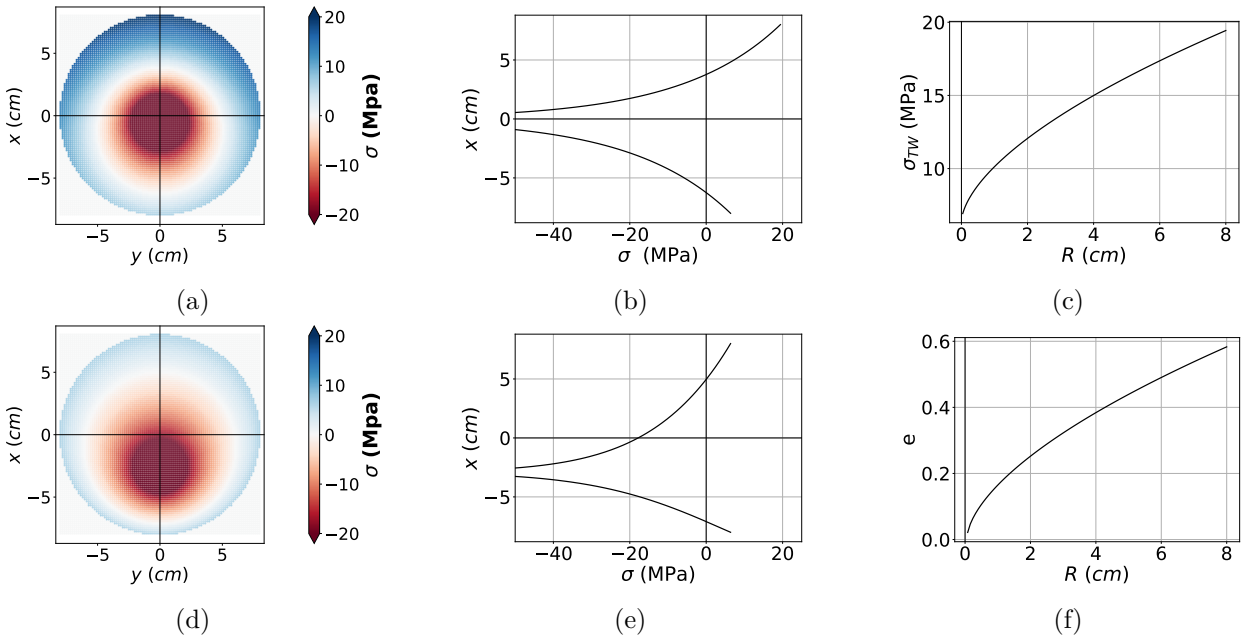

Figure 5: *Prunus avium*: The horizontal orientation of the branch is maintained by the two different processes: (a-c) the maturation stress provided by the formation of RW; (d-f) the eccentric growth; (a,d) 2D visualisation of the growth stress in the whole section; (b,e) Growth stress profile on diameter y=0. (c,f) Parametric representation of the tropic driver, maturation stress (c) and eccentricity (f).

Pinus pinaster

For *Pinus pinaster*, we used the same approach. The set of results is presented in Fig 7 and Fig 8. When no eccentricity was involved (Fig 7.a-c), a light compression stress was observed on the lower side of the section. When the branch grew, the compression stress increased (Fig 7.c). In case of no RW formation (i.e. homogeneous maturation stress), the distributions of growth stress and eccentricity (Fig 7.d-f) were quiet similar to the previous example with the birch tree: tension in periphery, compression near the pith, and an increasing eccentricity with branch growth.

The combination of the two factors is shown in Fig 8. As for *Prunus avium*, different eccentricities were imposed (Fig 8.a): the more epitrophic the eccentricity, the higher RW maturation stress. Although the different compression stress levels were close, the dynamic of this stress within the growth of the branch was different (Fig 8.a.ii). Also, the stress pattern exhibits a difference near the pith (Fig. 8.a.i), with some tension in this area for eccentricity $e = 0.5$. In case of a uniform RW maturation (8.b), the profile remained quite similar to birch tree. We could not impose a too low compression stress because of the above-mentioned coordination incompatibility.

Influence of branch orientation: the stationarity hypothesis

In order to evaluate the relevance of the stationarity hypothesis i.e. the branch keeps the same orientation, different growth scenarii were considered. For each branch, the case of active up-righting or passive bending was modelled (using equation 17). Passive bending was driven by increasing weight, calculated on the modelled branches. Up-righting was driven by the maturation gradient, which was set at 400 μstrain ($\sigma \approx 3.2$ MPa) for pine and 700 μstrain ($\sigma \approx 6.2$ MPa) for birch (the gradient was of the order of magnitude of NW stress). The results are shown in Fig 9. In birch, no major change of the stress pattern was observed. In contrast, the pattern changed greatly for pine. For a passive-bending branch, a 'V' profile and the absence of CW were observed. For up-righting, the previously-mentioned profile with tension at

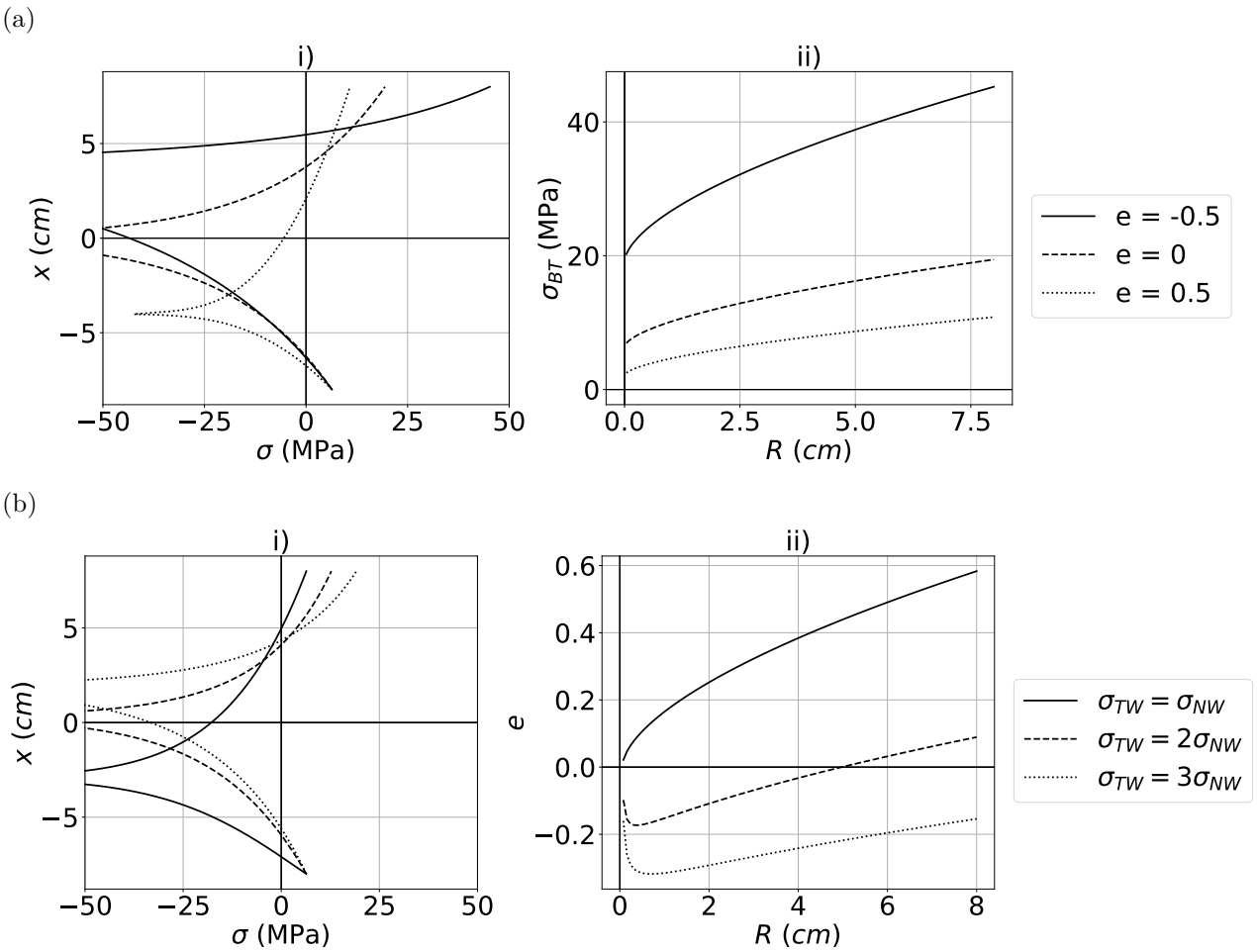

Figure 6: Different possible options to maintain the orientation of *Prunus avium* branches: (a) a constant eccentricity combined with the maturation that becomes the main driver of postural control; or (b) a constant maturation gradient combined with an eccentricity that becomes the main driver of postural control.

the pith was observed.

Discussion

Prunus avium: heavily loaded hardwood

Regarding the stress distribution (Fig 5), using either eccentric growth or RW led to realistic orders of magnitude (except near the pith, which is an intrinsic limit of our model. This specific point is discussed in section *Limits of the model*). In the case with no eccentricity, a tensile strain of $\mu_{RW} \approx 2140\mu$strain ($\sigma_{TW} \approx 19.5$ MPa) was obtained, quite similar to literature values, for much smaller branches: on 4 cm plagiotropic branches of eight tree species, Tsai et al. (2012) reported an average strain in RW of around 2100μstrain, with some values up to $\approx 5000\mu$strain. When combined with uniform eccentricity (Fig 6.a), it seems safer to promote the growth on the upper side: it minimises both high tensile stress and area with high compression stress. Interestingly, the worst case (hypotrophic eccentricity $e = -0,5$, more, solid line in Fig 6.a) led to levels approaching the limits, but previously observed [Huang et al. (2005); Tsai et al. (2012)]: $\mu_{RW} \approx 4970\mu$strain ($\sigma_{TW} \approx 45.4$ MPa)). Note that although for softwoods, there is a consensus on the usually observed eccentricity orientation (hypotrophic) [Timell (1986)], the eccentricity

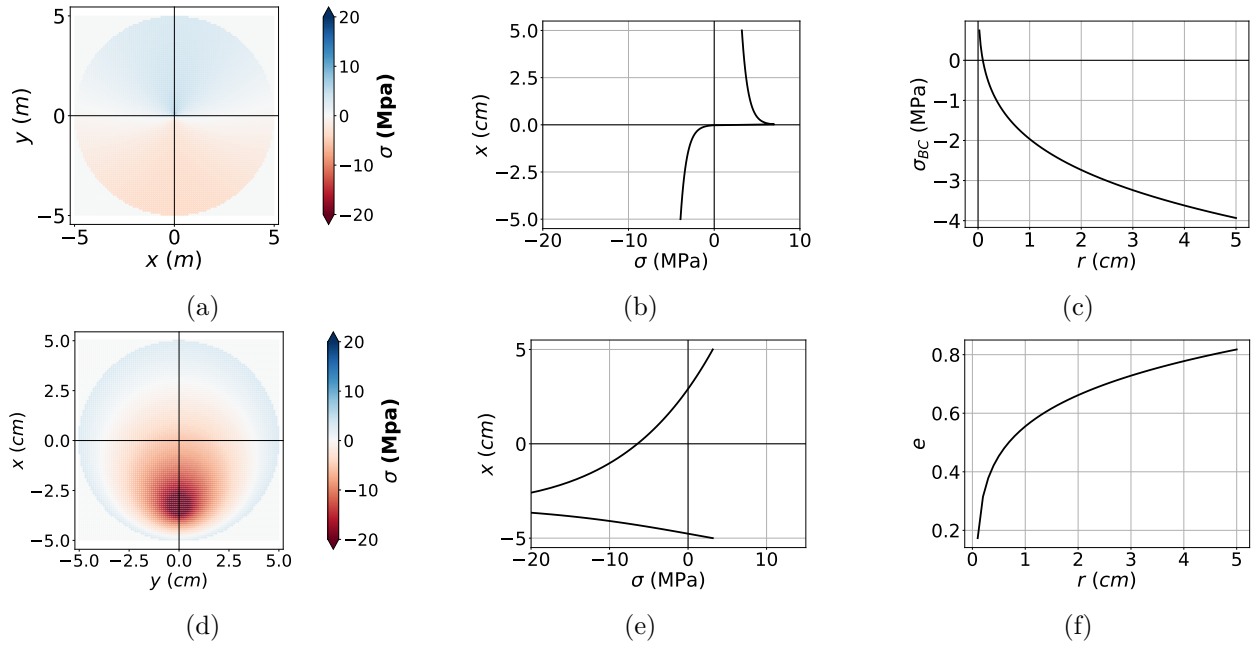

Figure 7: *Pinus pinaster*: The horizontal orientation of the branch is maintained by the two different processes: (a-c) the maturation stress provided by the formation of RW; (d-f) the eccentric growth; (a,d) 2D visualisation of the growth stress in the whole section; (b,e) Growth stress profile on diameter y=0. (c,f) Parametric representation of the tropic driver, maturation stress (c) and eccentricity (f).

has been observed in both directions in hardwood branches [Kucera and Philipson (1977); Wang et al. (2009b); Tsai et al. (2012)] although not usually in trunk. Therefore, this could be a tropic response for angiosperms branches, that tend to bend forward. This non-optimal pattern would be the consequence of a coordination between eccentricity and maturation stress. An extensive measurement campaign on branches would be needed to clarify this point. In the absence of RW (Fig 5.d-f), the eccentricity alone ensured the orientation. The maximal value was around 0.6, which seems quite high compared to literature values. For example, Hung et al. (2017) performed measurements on 10 plagiotropic branches of *Koelreuteria henryi*. The average radius was 2.6 cm, and the eccentricity had an average value of -0.37, with a maximum at -0.54. Unpublished data on more than 150 branches from six different temperate species showed very different patterns, depending from the species, but eccentricity was never below -0.5. This suggests that eccentricity is a limited driver of postural control. This result is in line with the work of Alméras et al. (2005), who showed that eccentricity in leaning stem explains a much lower part of the curvature than the maturation gradient ($\approx 29\%$ for eccentricity while $\approx 66\%$ for maturation gradient).

The combination of radial growth eccentricity with uniform maturation stress showed the same tendency as the dual combination (uniform eccentricity): a higher maturation stress led to a larger eccentricity. Comparing all simulations, the most optimal case was a constant positive eccentricity (dotted line in Fig 6.a). However, experimental observation showed that this is not the usual configuration for branches. It raises interesting question on the main mechanical driver of branch construction. From a biological point a view, it could be more "costless" to produce TW than eccentricity, but this hypothesis was not yet investigated. Also, more work is needed to understand how TW and eccentricity are linked in angiosperm trees: since they may have some uncoordinated action, we can wonder if they have common triggered factors.

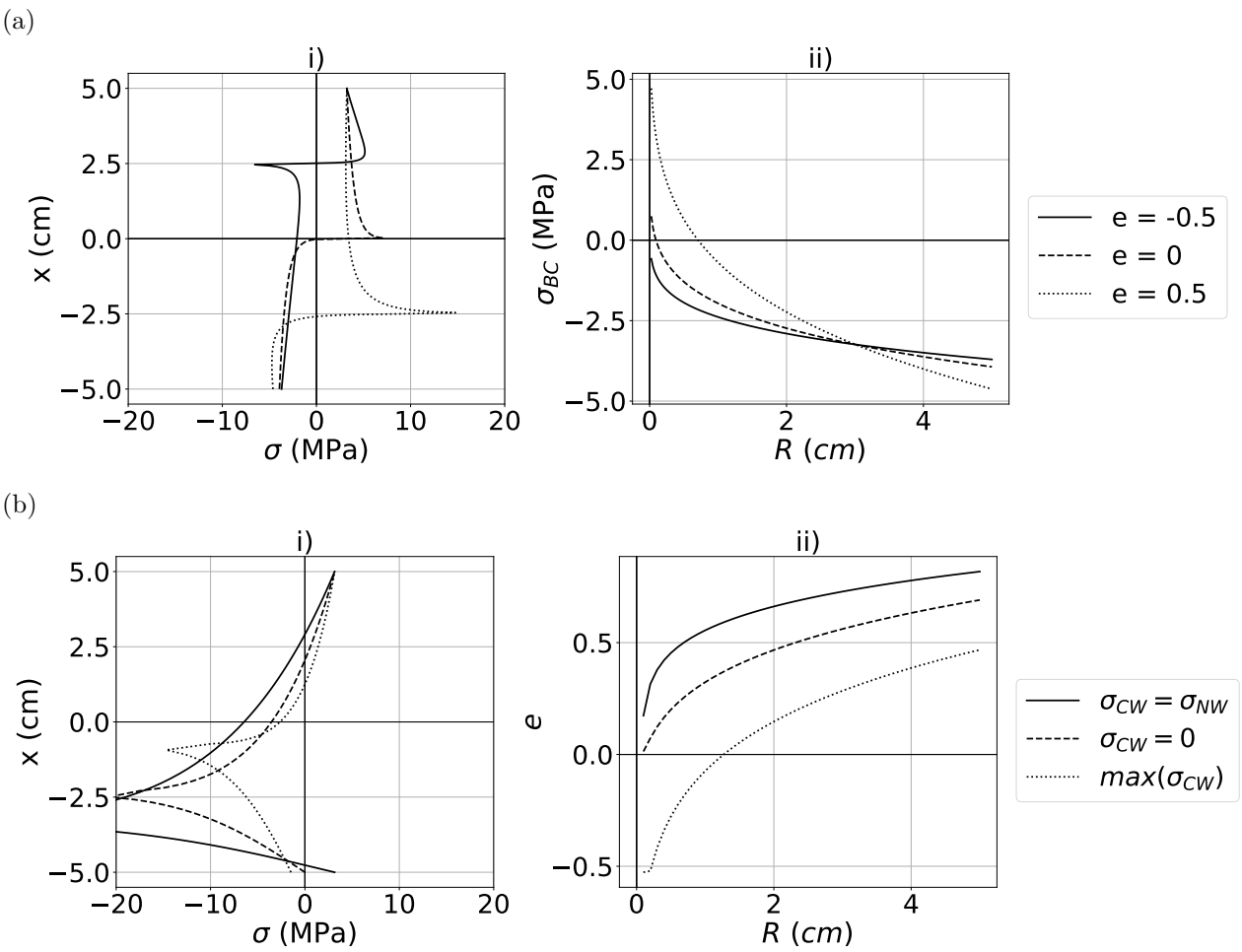

Figure 8: Different possible options to maintain the orientation of *Pinus pinaster* branches: (a) a constant eccentricity combined with the maturation that becomes the main driver of postural control; or (b) a constant maturation gradient combined with an eccentricity that becomes the main driver of postural control.

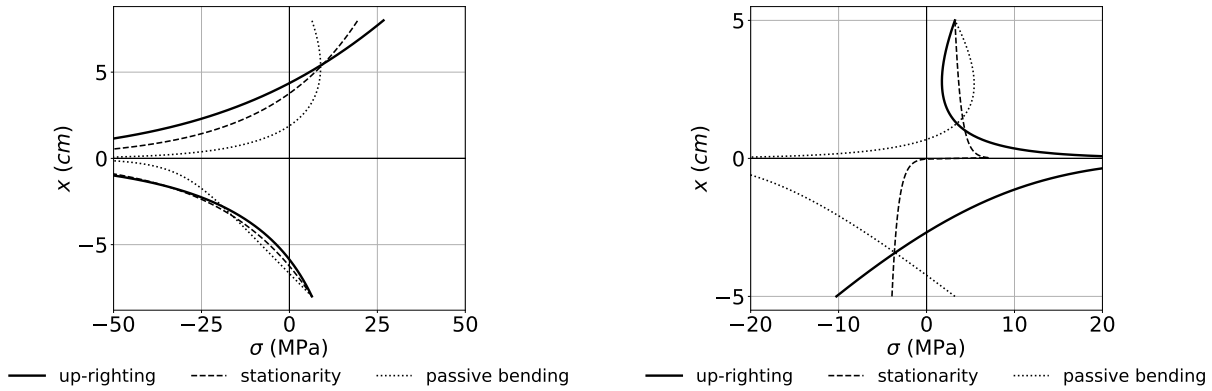

(a) Prunus

(b) Pinus

Figure 9: Distribution of growth stresses for different orientation scenarios.

***Pinus pinaster*: lightly loaded softwood**

First of all, the values of the stress distribution were much lower than for *Prunus avium.* This was explained by the size of the modelled branches: the average bending moment is much higher for birch

tree than for pine, by a factor roughly 10 (see λ_M and λ_N in Table 2). The effect of each factor alone (Fig 7) suggested that maturation is a much more efficient option than eccentricity. To ensure the same growth scenario, the eccentricity alone rose to about 0.8, which is close to a theoretical limit, whereas maturation alone led to low maturation strains in CW (<500 μstrain, corresponding to 4 MPa). Besides, this eccentricity was not in the direction of what is commonly observed. This point remains logical, because without CW, the epitrophic eccentricity is the only way to counteract the effect of gravity.
A uniform eccentricity combined with RW formation led to quite similar patterns (Fig 8.a): for this range of loading, the eccentricity had little influence on stress distribution.Considering that the density of elastic energy is proportional to the square of the stress, the pattern produced a low level of stored elastic energy, possibly reducing the risk of mechanical failure. Also, although eccentricity did not bring much variations in the value of the maturation stress, it considerably modified the shape of the resulting stress profiles (Fig 8.a.i). Indeed, these profiles can become 'crenellated' (Fig 8.a.i, dashed curve for zero eccentricity, solid curve for $e = -0.5$) or include tension at the pith (dotted line for $e = 0.5$). It seems that before producing tension in the pith, an efficient configuration could be reached by generating compression below the pith and tension above. Ideally, this may be a very relevant option for branches. These results about the mechanical strategies of branches should be confronted to experimental measurements. Otherwise, these pattern changes could also be an optimisation of the residual strength of wood: CW is known to have high compressive strength conferred by its high lignin content and cell wall structure. Generating some tension at the pith allows the branch to create more CW. To answer this question it would be necessary to take into account strength parameters in our stress computation model. Adding a damage-elastoplastic law would also allow to study the effects of stress relaxation and to observe if some profiles, that are here not optimal for maintaining the branch orientation, could possibly become optimal for resisting breakage.
Using eccentricity combined to RW formation (Fig 8.b) leads to usual patterns, with compression near the pith, tension on the upper side and compression on the lower one. Eccentricity is epitrophic: this is the opposite to what is usually observed: unpublished data on 20 branches (average radius of 3 cm) of *Pinus nigra* showed an average eccentricity of -0.2. This non-intuitive result is partly explained by our hypothesis of uniform stiffness, as will be discussed later.It is also explained here by the change of sign between NW and CW. In the early stages of growth, as long as the stress in the CW is lower than in the NW, the best option to maintain the orientation is to do epitrophic eccentricity. Once the stress in the CW becomes higher than in the NW, it is more efficient to do hypotrophic eccentricity. Our scenarios do not allow us to reach stress levels in compression that are higher than the stress in normal wood. This is due to the above mentioned incompatibility of our scenario.

Influence of the branch's orientation : the stationary hypothesis

In both trees, the orders of magnitude are compatible with a mechanical safety margin for the branches. Apart from modified tropisms (change of light environment, weight change by loss of part of the branch, etc.), the maintaining of the orientation is quite common for real branches. However our simulations suggest that if, for any reason, they need to modify their orientation, they can do it without taking too much mechanical risk. The hypothesis of branch direction stationarity is totally in accordance with the long-term mechanical requirements needed during the construction of branches.

Vertical bending moment vs horizontal bending and torsion moments

One of the hypothesis of our model was that the vertical bending moment (M_y) prevails over the torsional M_z and horizontal bending M_x moments. This allowed to consider only one direction of eccentricity and to avoid all the non-linear terms generated by the torsional components. We evaluated the maximum values of the three moments for all modelled branches of each species for comparison purpose. The results are presented in Fig 10. They enlighten that for each species, the vertical moment shows much higher values than the torsional and horizontal bending moments and validates our initial hypothesis.

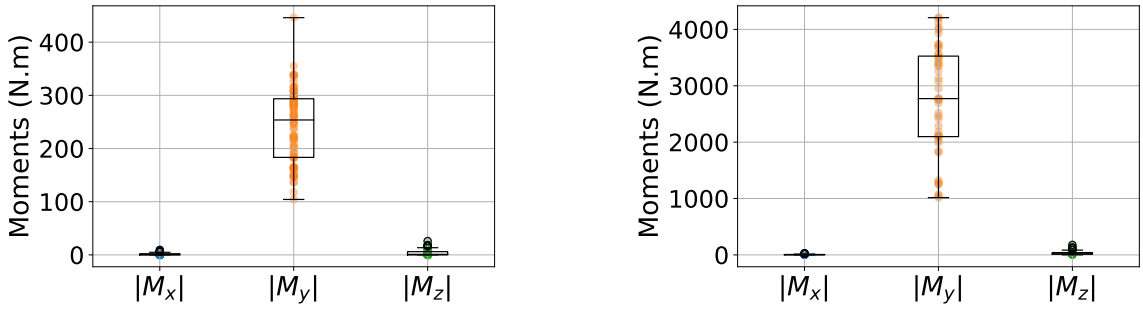

(a) Pinus

(b) Prunus

Figure 10: Comparison of maximum moments for modelled branches. Mx: horizontal moment; My: vertical moment; Mz: torsional moment.

Limits of the model

The hypothesis of homogeneous wood stiffness in the whole section is questionable. Systematic stiffness differences have been observed between wood types (TW or CW vs NW). Alméras et al. (2005) have studied the variation of Young's modulus in the section of leaning stems from 14 angiosperms and 3 gymnosperms, all coming from different families. For the angiosperms, the average Young's modulus of TW was higher than in NW by 15%, while for the gymnosperms, the Young's modulus was 38% lower in CW than in NW. This heterogeneity of rigidity plays a role in the postural control of the stems [Alméras et al. (2005); Huang et al. (2010); Hung et al. (2017)]. In our case, either a higher rigidity in TW or a lower in CW would make the branch bend upward. In the current formulation of the model imposing an homogeneous stiffness, an almost equivalent effect would have been obtained by an initial offset in the eccentricity. Calling this offset tentatively 'compensating eccentricity' e_c (Fig 11), the model computed a total eccentricity, e, combining e_c and the "real" eccentricity needed to maintain the orientation. Therefore, in case in RW formation on one side, the eccentricity displayed need to be offset by e_c to correspond to more realistic situations. This explains, for instance, why the simulations for the softwood resulted in hypertrophic eccentricity while it is well-known that inclined softwood stems usually exhibit hypotropic eccentricity. Although data are missing to approximate the value of this parameter, and further work is needed to assess theoretically the possible equivalence between rigidity variations and eccentricity, the available information on relative stiffness of NW and RW suggests a more important effect in gymnosperms than in angiosperms.

The evaluation of the stress during the first stages of branch development is ano issue of the model. In almost every stress profile, a tension or compression peak is generated in the pith. It generally exceeds the wood strength, which is not compatible with branch sustainability. This point could be corrected in two ways. First, the role of the bark could be taken into account. Its mechanical role for small axes has already been studied and its importance in postural maintenance was clearly highlighted [Clair et al. (2019); Ghislain et al. (2019)]. Our model could include the mechanical action of bark in the early stages of branch development. This improvement would require additional data about the mechanical behaviour of the bark but would bring more realistic stress predictions and limit the artefacts at the pith. A second exciting perspective would be to take into account the elastoplastic behaviour of wood. By imposing a realistic plastic strain limit, the peak at the pith would then disappear; the increments would be spread over the middle part of the section, thus modifying the non-realistic patterns previously observed.

Finally, modelling the evolution of normal force and bending moment loads by allometric laws was questionable. Indeed, the orientation of the branch may vary with time, which implies variations of the effect of weight. For example, modelling a constant increase of the normal force is inappropriate if the inclination of the branch decreases with time. An improvement of our model could be the construction

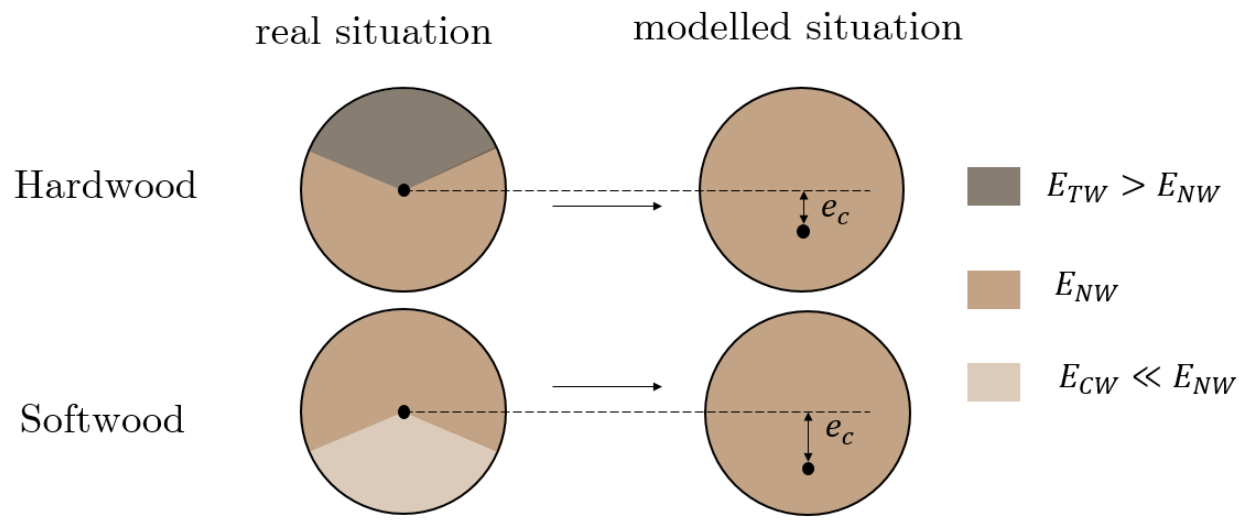

Figure 11: How the hypothesis of a uniform wood stiffness impacts the initial position of the pith.

of loads based on equivalent length allometries taking into account the mass of the branch, and the computation of the loads for each position in the right reference frame.

Conclusion and perspectives

A semi-analytical growth stress model has been developed in the context of branch development. At each radius increment, the stress balance is computed in order to fit with a fixed curvature. A first novelty of this model is that it takes into account the role of the eccentricity variation over the years. A second contribution is the computation of stress distribution in the whole cross-section. We tested the effectiveness of two well-known biomechanical processes of woody plants to control the orientation of their axes: eccentric radial growth and RW formation. The case of one softwood *Pinus pinaster* and one hardwood *Prunus avium* were computed using data provided by AMAPSim software. For both trees, growth stress simulations showed that maturation stress was more efficient than eccentric radial growth to maintain a fixed orientation (i.e. to counter the increasing gravity constrain applied to the growing branch). For the hardwood branches, the computations highlighted that the eccentricity needed to maintain orientation did not corroborate the observations reported in literature. This suggests that this parameter probably provides another function than the orientation control, like the improved bending strength of the branch that provides it a greater mechanical safety. For the softwood branches, although the model showed that eccentric radial growth did not play a major role in maintaining the branch's orientation, it does modify the shape of the stress profiles in the cross section of the branch. A few odd and critical profiles, crenellated or with tension near the pith, have been identified. Their analysis provided exciting perspectives for further experimental works to gather real data.

Now that a complete model is available, it becomes crucial to start experimental investigations on branches in order to compare the outputs with real in situ observations. Especially, we need to evaluate the relevance of the different biological processes used by branches to ensure their mechanical sustainability over the years.

From a biological point of view, a key point for understanding branch sizing is the question of biomass costs. Building additional wood on one side or forming RW are carbon sinks with possible trade-offs. In order to investigate this point, our model could help by affecting a cost to the production of RW as well as to eccentric growth. The resulting computations could then help to understand the relevance of some options and would lead to coupling the biomechanical point of view to other biological considerations.

References

T. Alméras, D. Jullien, and J. Gril. *Modelling, Evaluation and Biomechanical Consequences of Growth Stress Profiles Inside Tree Stems*, pages 21–48. Springer International Publishing, Cham, 2018. ISBN 978-3-319-79099-2. doi: 10.1007/978-3-319-79099-2_2. URL https://doi.org/10.1007/978-3-319-79099-2_2.

T. Alméras and B. Clair. Critical review on the mechanisms of maturation stress generation in trees. *Journal of The Royal Society Interface*, 13(122):20160550, 2016. doi: 10.1098/rsif.2016.0550. URL https://royalsocietypublishing.org/doi/abs/10.1098/rsif.2016.0550.

T. Alméras and M. Fournier. Biomechanical design and long-term stability of trees: Morphological and wood traits involved in the balance between weight increase and the gravitropic reaction. *Journal of Theoretical Biology*, 256(3):370–381, 2009. ISSN 0022-5193. URL http://www.sciencedirect.com/science/article/pii/S0022519308005389.

T. Alméras, A. Thibaut, and J. Gril. Effect of circumferential heterogeneity of wood maturation strain, modulus of elasticity and radial growth on the regulation of stem orientation in trees. *Trees*, 19(4):457–467, 2005. ISSN 1432-2285. URL https://doi.org/10.1007/s00468-005-0407-6.

P. Ancelin, T. Fourcaud, and P. Lac. Modelling the biomechanical behaviour of growing trees at the forest stand scale. part i: Development of an incremental transfer matrix method and application to simplified tree structures. *Annals of Forest Science*, 61(3):263–275, 2004.

R. R. Archer. On the distribution of tree growth stresses. ii. stresses due to asymmetric growth strains. *Wood Science and Technology*, V10:293–309, 1976.

R. R. Archer and F. E. Byrnes. On the distribution of tree growth stresses – part i: An anisotropic plane strain theory. *Wood Science and Technology*, 8(3):184–196, 1974. ISSN 1432-5225. URL https://doi.org/10.1007/BF00352022.

J.-F. Barczi, H. Rey, Y. Caraglio, P. de Reffye, D. Barthélémy, Q. X. Dong, and T. Fourcaud. AmapSim: A Structural Whole-plant Simulator Based on Botanical Knowledge and Designed to Host External Functional Models. *Annals of Botany*, 101(8):1125–1138, 09 2007. ISSN 0305-7364. doi: 10.1093/aob/mcm194. URL https://doi.org/10.1093/aob/mcm194.

D. Barthélémy, Y. Caraglio, and S. Sabatier. 4.1 crown architecture of valuable broadleaved species. *Valuable broadleaved forests in Europe*, 22:87, 2009.

D. Barthélémy and Y. Caraglio. Plant Architecture: A Dynamic, Multilevel and Comprehensive Approach to Plant Form, Structure and Ontogeny. *Annals of Botany*, 99(3):375–407, 01 2007. ISSN 0305-7364. doi: 10.1093/aob/mcl260. URL https://doi.org/10.1093/aob/mcl260.

Y. Caraglio. Le développement architectural du merisier. *Forêt Entreprise 107*, (107):72–80, 1996.

B. Clair, B. Ghislain, J. Prunier, R. Lehnebach, J. Beauchêne, and T. Alméras. Mechanical contribution of secondary phloem to postural control in trees: the bark side of the force. *New Phytologist*, 221(1):209–217, 2019. doi: https://doi.org/10.1111/nph.15375. URL https://nph.onlinelibrary.wiley.com/doi/abs/10.1111/nph.15375.

T. Coudurier, D. Barthelemy, B. Chanson, F. Courdier, and C. Loup. Premier résultats sur la modélisation du pin maritime pinus pinaster ait.(pinecae). *Architecture des arbres fruitiers et forestiers*, page 306, 1993.

C. Coutand, M. Fournier, and B. Moulia. The gravitropic response of poplar trunks: Key roles of prestressed wood regulation and the relative kinetics of cambial growth versus wood maturation. *Plant Physiology*, 144(2):1166–1180, 2007. ISSN 0032-0889. doi: 10.1104/pp.106.088153. URL http://www.plantphysiol.org/content/144/2/1166.

476 J. B. Fisher and J. W. Stevenson. Occurrence of reaction wood in branches of dicotyledons and its
477 role in tree architecture. *Botanical Gazette*, 142(1):82–95, 1981. doi: 10.1086/337199. URL `https:`
478 `//doi.org/10.1086/337199`.

479 T. Fourcaud, F. Blaise, P. Lac, P. Castéra, and P. de Reffye. Numerical modelling of shape regulation and
480 growth stresses in trees. *Trees*, 17(1):31–39, 2003. ISSN 1432-2285. URL `https://doi.org/10.1007/`
481 `s00468-002-0203-5`.

482 M. Fournier, B. Chanson, D. Guitard, and B. Thibault. Mécanique de l'arbre sur pied : modélisation d'une
483 structure en croissance soumise à des chargementspermanents et évolutifs. 1. analyse des contraintes de
484 support. 1991a.

485 M. Fournier, B. Chanson, D. Guitard, and B. Thibault. Mécanique del'arbre sur pied :modélisation d'une
486 structure en croissance soumise à des chargements permanents et évolutifs.2. analyse tridimensionnelle
487 des contraintesde maturation, cas du feuillu standard. 1991b.

488 M. Fournier, H. Baillères, and B. Chanson. Tree biomechanics : growth, cumulative prestresses, and
489 reorientations. *Biomimetics*, 2(3):229–251, 1994.

490 B. Ghislain, T. Alméras, J. Prunier, and B. Clair. Contributions of bark and tension wood and role of the
491 g-layer lignification in the gravitropic movements of 21 tropical tree species. *Annals of Forest Science*,
492 76(4):107, 2019. ISSN 1297-966X. URL `https://doi.org/10.1007/s13595-019-0899-7`.

493 J. Gérard, D. Guibal, S. Paradis, M. Vernay, J. Beauchêne, L. Brancheriau, I. Châlon, C. Daigremont,
494 P. Détienne, D. Fouquet, P. Langbour, S. Lotte, M.-F. Thévenon, C. Méjean, and A. Thibaut. Tropix 7,
495 2011. URL `http://tropix.cirad.fr/en`.

496 F. Hallé, R. A. Oldeman, and P. B. Tomlinson. *Tropical trees and forests: an architectural analysis*.
497 Springer Verlag, 1978.

498 P. Heuret, C. Meredieu, T. Coudurier, F. Courdier, and D. Barthélémy. Ontogenetic trends in the
499 morphological features of main stem annual shoots of pinus pinaster (pinaceae). *American Journal of*
500 *Botany*, 93(11):1577–1587, 2006. doi: https://doi.org/10.3732/ajb.93.11.1577. URL `https://bsapubs.`
501 `onlinelibrary.wiley.com/doi/abs/10.3732/ajb.93.11.1577`.

502 Y.-S. Huang, S.-S. Chen, L.-L. Kuo-Huang, and C.-M. Lee. Growth strain in the trunk and branches of
503 chamaecyparis formosensis and its influence on tree form. *Tree Physiol*, 25(9):1119–1126, Sept. 2005.
504 ISSN 0829-318X. URL `https://doi.org/10.1093/treephys/25.9.1119`.

505 Y.-S. Huang, L.-F. Hung, and L.-L. Kuo-Huang. Biomechanical modeling of gravitropic response of
506 branches: roles of asymmetric periphery growth strain versus self-weight bending effect. *Trees*, 24(6):
507 1151–1161, 2010. ISSN 1432-2285. URL `https://doi.org/10.1007/s00468-010-0491-0`.

508 L.-F. Hung, C.-C. Tsai, S.-J. Chen, Y.-S. Huang, and L.-L. Kuo-Huang. Study of tension wood in
509 the artificially inclined seedlings of koelreuteria henryi dummer and its biomechanical function of
510 negative gravitropism. *Trees*, 30(3):609–625, 2016. ISSN 1432-2285. URL `https://doi.org/10.1007/`
511 `s00468-015-1304-2`.

512 L.-F. Hung, C.-C. Tsai, S.-J. Chen, Y.-S. Huang, and L.-L. Kuo-Huang. Strain distribution, growth
513 eccentricity, and tension wood distribution in the plagiotropic and orthotropic branches of koelreuteria
514 henryi dummer. *Trees*, 31(1):149–164, 2017. ISSN 1432-2285. URL `https://doi.org/10.1007/`
515 `s00468-016-1464-8`.

516 L. J. Kucera and W. R. Philipson. Growth eccentricity and reaction anatomy in branchwood of drimys
517 winteri and five native new zealand trees. *New Zealand Journal of Botany*, 15(3):517–524, 1977. doi:
518 10.1080/0028825X.1977.10429625. URL `https://doi.org/10.1080/0028825X.1977.10429625`.

H. Kübler. Studien über wachstumsspannungen des holzes iii. längenänderungen bei der wärmebehandlung frishen holzes. *Holz Rohst Werkst*, 17(3):77–86, 1959.

J. E. Nicholson. A rapid method for estimating longitudinal growth stresses in logs. *Wood Science and Technology*, 5(1):40–48, 1971. ISSN 1432-5225. URL https://doi.org/10.1007/BF00363119.

B. Thibaut. Three-dimensional printing, muscles, and skeleton: mechanical functions of living wood. *Journal of Experimental Botany*, 70(14):3453–3466, 04 2019. ISSN 0022-0957. doi: 10.1093/jxb/erz153. URL https://doi.org/10.1093/jxb/erz153.

B. Thibaut and J. Gril. Tree growth forces and wood properties. *Peer Community Journal*, 1:e46, 2021. doi: 10.24072/pcjournal.48. URL https://peercommunityjournal.org/articles/10.24072/pcjournal.48/.

T. E. Timell. *Compression wood in gymnosperms*, volume 1. Springer, 1986.

C.-C. Tsai, L.-F. Hung, C.-T. Chien, S.-J. Chen, Y.-S. Huang, and L.-L. Kuo-Huang. Biomechanical features of eccentric cambial growth and reaction wood formation in broadleaf tree branches. *Trees*, 26 (5):1585–1595, 2012. ISSN 1432-2285. URL https://doi.org/10.1007/s00468-012-0733-4.

Y. Wang, J. Gril, and J. Sugiyama. Variation in xylem formation of viburnum odoratissimum var. awabuki: growth strain and related anatomical features of branches exhibiting unusual eccentric growth. *Tree Physiol*, 29(5):707–713, May 2009a. ISSN 0829-318X. URL https://doi.org/10.1093/treephys/tpp007.

Y. Wang, J. Gril, and J. Sugiyama. Is the branch of viburnum odoratissimum var. awabuki reaction wood? unusual eccentric growth and various distributions of growth strain. In *6th Plant Biomechanics Conference*, pages 328–334, 2009b.

H. Yamamoto, M. Yoshida, and T. Okuyama. Growth stress controls negative gravitropism in woody plant stems. *Planta*, 216(2):280–292, 2002. ISSN 1432-2048. URL https://doi.org/10.1007/s00425-002-0846-x.

J. L. Yang, H. Baillères, T. Okuyama, A. Muneri, and G. Downes. Measurement methods for longitudinal surface strain in trees: a review. *Australian Forestry*, 68(1):34–43, 2005. doi: 10.1080/00049158.2005.10676224. URL https://doi.org/10.1080/00049158.2005.10676224.

M. Yoshida and T. Okuyama:. Techniques for measuring growth stress on the xylem surface using strain and dial gauges. 56(5):461–467, 2002. doi: doi:10.1515/HF.2002.071. URL https://doi.org/10.1515/HF.2002.071.

Appendix A

The calculation of integrals of system (3) requires preliminary elements. The situation of two consecutive rings is represented in Fig. 12. Each position x in the geometrical reference frame is expressed with respect to the position x' in the pith reference frame according to the equation:

$$x = r\cos\theta = x' - \overline{e}R \tag{24}$$

with r the radius at time t and R the radius at the final time.

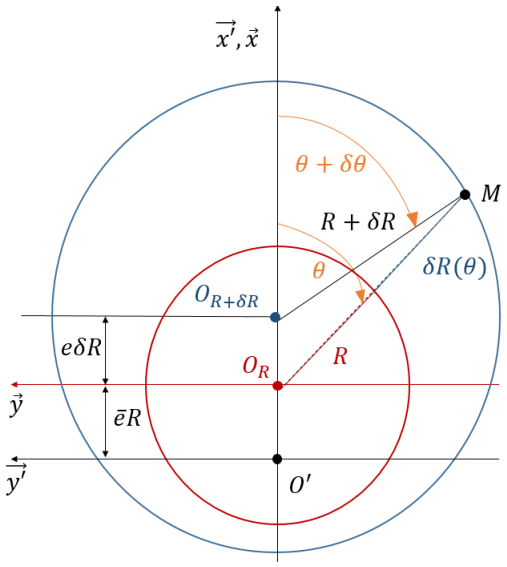

Figure 12: Representation of two consecutive rings and the elements needed to calculate $\delta R(\theta)$

The integrals of system (3) are computed as follows:

$$\begin{aligned}
\int_s \delta\sigma ds &= \int_s E\left[\delta a + (x + \overline{e}.R)\delta b\right] r\delta r d\theta \\
&= E\pi R^2\left(\delta a + \overline{e}.R\delta b\right) \\
\int_s x'\delta\sigma ds &= \int_s \left[\delta a + (x + \overline{e}.R)\delta b\right]\left[x + \overline{e}.R\right] r\delta r d\theta \\
&= E\pi R^3\left[\overline{e}\delta a + R\left(\overline{e}^2 + \frac{1}{4}\right)\delta b\right]
\end{aligned}$$

The tangential distribution of the radius increment $\delta R(\theta)$ is required to compute the maturation terms. Applying $\overrightarrow{O_R M} - \overrightarrow{O_{R+dR}M} = \overrightarrow{O_R O_{R+dR}}$ (Fig 12):

$$\begin{cases}
\left[R + \delta R(\theta)\right]\cos\theta - (R + \delta R)\cos(\theta + \delta\theta) = e_R\delta R & \text{(25a)} \\
\left[R + \delta R(\theta)\right]\sin\theta - (R + \delta R)\sin(\theta + \delta\theta) = 0 & \text{(25b)}
\end{cases}$$

By setting $\delta\theta \to 0$, it comes:

$$\begin{cases}
\cos(\theta + \delta\theta) = \cos\theta - \sin\theta\delta\theta & \text{(26a)} \\
\sin(\theta + \delta\theta) = \sin\theta + \cos\theta\delta\theta & \text{(26b)}
\end{cases}$$

Substituting (26) into (25), and combining (25a) and (25b), $\delta R(\theta)$ can finally be written as:

$$\boxed{\delta R(\theta) = \delta R\left[1 + e_R \cos\theta\right]} \tag{27}$$

Then:

$$\begin{aligned}
\int_{\delta s} \sigma_0^i ds &= \int_{\delta s} \sigma_0^i(\theta) R\delta R(\theta) d\theta \\
&= \int_{\delta s} \left[\alpha + \beta\cos\theta\right]\left[1 + e\cos\theta\right] R\delta R(\theta) d\theta \\
&= \pi\left(2\alpha + e\beta\right) R\delta R \\
\int_{\delta s} x'\sigma_0^i ds &= \int_{\delta s} \sigma_0^i(\theta)(x + e.R) R\delta R(\theta) d\theta \\
&= R^2\delta R\pi\left(3\alpha e + \beta e^2 + \beta\right)
\end{aligned}$$

Appendix B

The matrix system (7) becomes:

$$\begin{cases}
\delta a = \dfrac{\delta F_0 K_2 - \delta F_1 K_1}{K_0 K_2 - K_1^2} & \text{(28a)} \\
\delta b = \dfrac{\delta F_0 K_1 - \delta F_1 K_0}{K_1^2 - K_0 K_2} & \text{(28b)}
\end{cases}$$

Then, numerators and denominators are calculated separately:

$$K_0 K_2 - K_1^2 = E^2\pi^2 R^6\left(\overline{e}^2 + \frac{1}{4}\right) - E^2\pi^2 R^6\overline{e}^2 = \frac{\left(E\pi R^3\right)^2}{4}$$

$$\begin{aligned}
\delta F_0 K_2 - \delta F_1 K_1 &= E\pi^2 R^5\left[-\left(2\alpha + e\beta\right)\left(\overline{e}^2 + \frac{1}{4}\right) + \overline{e}\left(3\alpha e + \beta e^2 + \beta\right)\right]\delta R + E\pi R^3\left[R\delta N\left(\overline{e}^2 + \frac{1}{4}\right) + \overline{e}\delta M\right] \\
&= E\pi^2 R^5\left[\alpha\left(3e\overline{e} - 2\overline{e}^2 - \frac{1}{2}\right) + \beta\left(\overline{e}e^2 - e\overline{e}^2 + \overline{e} - \frac{e}{4}\right)\right]\delta R + E\pi R^3\left[R\delta N\left(\overline{e}^2 + \frac{1}{4}\right) + \overline{e}\delta M\right]
\end{aligned}$$

$$\begin{aligned}
\delta F_0 K_1 - \delta F_1 K_0 &= E\pi^2 R^4\left[-\overline{e}\left(2\alpha + e\beta\right) + \left(3\alpha e + e^2\beta + \beta\right)\right]\delta R + E\pi R^2\left[\overline{e}R\delta N + \delta M\right] \\
&= E\pi^2 R^4\left[\alpha\left(3e - 2\overline{e}\right) + \beta\left(1 + e^2 - e\overline{e}\right)\right]\delta R + E\pi R^2\left[\overline{e}R\delta N + \delta M\right]
\end{aligned}$$

Putting the calculations together, system (28) becomes:

$$\begin{cases}
\delta a = \dfrac{4}{ER}\left[\alpha\left(3e\overline{e} - 2\overline{e}^2 - \dfrac{1}{2}\right) + \beta\left(\overline{e}e^2 - e\overline{e}^2 + \overline{e} - \dfrac{e}{4}\right)\right]\delta R + \dfrac{4}{E\pi R^3}\left[R\delta N\left(\overline{e}^2 + \dfrac{1}{4}\right) + \overline{e}\delta M\right] \\
\delta b = \dfrac{-4}{ER^2}\left[\alpha\left(3e - 2\overline{e}\right) + \beta\left(1 + e^2 - e\overline{e}\right)\right]\delta R + \dfrac{-4}{E\pi R^4}\left[\overline{e}R\delta N + \delta M\right]
\end{cases}$$

Appendix C

The following calculus is based on Fig 3.b. To get the vertical bending moment M_y of unit n (eq 23), one need the calculation of each volume V_n and center of gravity G_n. Let name $D(z)$ the diametral extension of the cone. It comes:

$$V_n = \int_0^{L_n} \frac{\pi D(z)^2}{4} dz \tag{30}$$

where $D(z) = D_n + \left(\frac{D_{n+1}-D_n}{L_n}\right) z$. One gives

$$O_n G_n = \frac{1}{V_n} \int_0^{L_n} \frac{\pi D(z)^2}{4} z dz \tag{31}$$

Setting $\gamma = \frac{D_{n+1}-D_n}{D_n}$ and $\xi = \frac{L_n}{z}$, equations (30) and (31) become:

$$V_n = \frac{\pi D_n^2 L_n}{4} \int_0^1 (1+\gamma\xi)^2 \, d\xi = \frac{\pi D_n^2 L_n}{4} . \left(1 + \gamma + \frac{\gamma^2}{3}\right)$$

$$O_n G_n = \frac{1}{V_n} \frac{\pi D_n^2 L_n^2}{4} . \left(\frac{1}{2} + \frac{2\gamma}{3} + \frac{\gamma^2}{4}\right)$$

So, finally, $O_n G_n$ can be written:

$$O_n G_n = \frac{L_n}{2} \left(\frac{1 + \frac{4}{3}\gamma + \frac{1}{2}\gamma^2}{1 + \gamma + \frac{1}{3}\gamma^2}\right) \tag{32}$$